Optics Communications 475 (2020) 126240

Contents lists available at ScienceDirect

Optics Communications

journal homepage: www.elsevier.com/locate/optcom

A side-ported MMI based InP polarization beam splitter

Qiang Tang, Yunlong Liu, Lichen Zhang, Xiaobo La, Xuyuan Zhu, Song Liang *, Lingjuan Zhao, Wei Wang

Key Laboratory of Semiconductor Materials Science, Institute of Semiconductors, Chinese Academy of Sciences, Beijing 100083, China
Beijing Key Laboratory of Low Dimensional Semiconductor Materials and Devices, Institute of Semiconductors, Chinese Academy of Sciences, Beijing 100083, China
Center of Materials Science and Optoelectronics Engineering, University of Chinese Academy of Sciences, Beijing 100049, China

ARTICLE INFO

Keywords:
Multimode interference (MMI)
Polarization beam splitter (PBS)
Side ported

ABSTRACT

The design of a multimode interference coupler (MMI) based InP polarization beam splitter (PBS) at 1.3 μm wavelength is reported. When the input and output waveguides are placed on the side walls of the PBS MMIs, the PBS can be shortened effectively, while maintaining both low insertion loss (IL) and high extinction ratio (ER). The optimized PBS design is 299 μm in length which is less than 1/3 of the PBS with end ported access ports. At the same time, the ER of the side ported PBS is notably better than the ER of the long end ported PBS.

1. Introduction

The polarization beam splitter (PBS), which is used to realize on-chip polarization control in a photonic integrated circuit, has been arousing great interests in recent years. A PBS enables polarization division multiplexing (PDM) in an optical communication system, which doubles the data capacity to meet the ever-increasing bandwidth demands of signal transmission [1]. In addition, through combination of the application of PBSs and polarization rotators, polarization transparency can be realized for photonic integrated circuits (PICs) [2]. Compared with Si based PICs, InP based PICs have the advantage that light sources can be integrated monolithically [1–3]. Besides PBSs on Si based PICs [4–6], InP based PBSs, which can be integrated with both passive and active optical components, have also been presented for InP PICs in recent years [7–10]. The design of PBS is generally based on two mechanisms including modal evolution and interferometry. The modal evolution-based PBS can be realized by combining an adiabatic mode-converter and an asymmetric Y-coupler [8]. The interferometry-based PBSs can be realized by using directional couplers (DC) [11,12], Mach–Zehnder interferometers (MZI) [13,14], and multimode interference couplers (MMI) [9,15]. Among these different types of PBSs, the MMI based PBSs have several advantages including low insertion loss, easy design and simple process of production, which have attracted a lot of attention from researchers.

In this paper, we report the design of a side-ported cascaded MMI based InP PBS at 1.31 μm wavelength. By placing the input and output waveguides on the side walls of the MMIs, the length of the PBS can be shortened effectively, while still maintaining both low insertion loss (IL) and high extinction ratio (ER). The results obtained from 3D BPM studies show that the length of the side-ported PBS is 299 μm, which is only 1/3 of the length of the PBS which has end ported access ports in Ref. [9]. For both TE and TM modes, extinction ratios (ER) are larger than 31 dB and insertion losses (IL) are smaller than 0.6 dB at 1310 nm.

2. Theory and simulation results

For the general type of interference, a reproduced self-image is located at:

$$L = m(3L_\pi) \quad with \quad (m = 1, 2, 3 \ldots) \tag{1}$$

where the factor m represents the periodic nature of the imaging along the MMI waveguide, and $3L_\pi$ is the self-imaging length given by:

$$3L_\pi = 3\frac{4n_r W_e^2}{3\lambda_0} \tag{2}$$

where L_π, n_r, W_e and λ_0 are the beat length of the lowest-order mode, the effective refractive index of the MMI, the width of the MMI, and the working wavelength. In our design, the factor m equals 1 which means the lengths of the MMIs equals their self-imaging lengths.

The propagations of lights of TE and TM modes in a side ported MMI are shown in Fig. 1(a) and (b), respectively. For TM polarization, the first order self-image is at L_{TM} on the right-boundary side. An output waveguide can be put there to couple the TM light power out. For TE polarization, its self-image is also located at L_{TE} on the right-boundary side, but it is smaller than L_{TM}. Due to the shorter self-imaging length of TE polarization, the TE light power is reflected at L_{TE} to the left side of the MMI before leaking into the TM output waveguide. As

* Corresponding author at: Qinghua East Road Jia #35, Beijing, China.
E-mail address: liangsong@semi.ac.cn (S. Liang).

https://doi.org/10.1016/j.optcom.2020.126240
Received 27 April 2020; Received in revised form 30 June 2020; Accepted 3 July 2020
Available online 4 July 2020

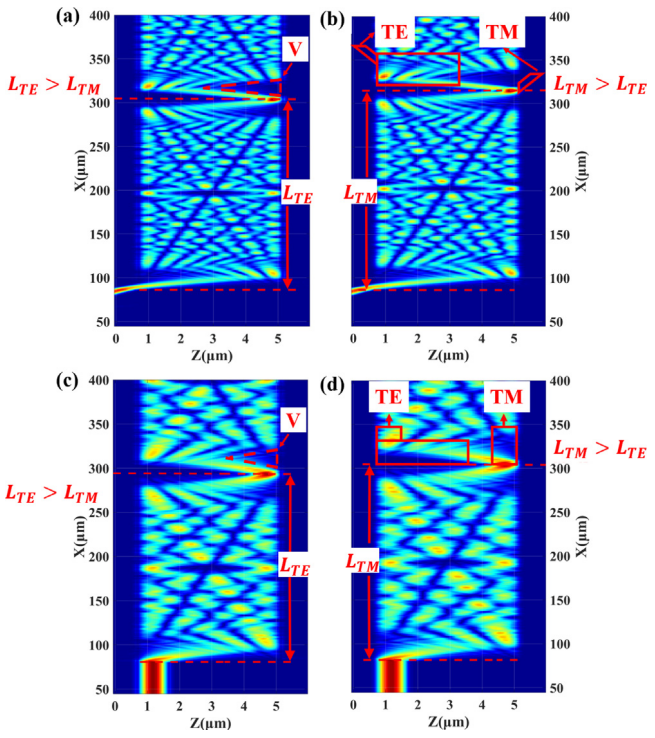

Fig. 1. Propagations of lights at 1310 nm in (a) quasi-TE mode, side ported MMI; (b) quasi-TM mode, side ported MMI; (c) quasi-TE mode, end ported MMI; (d) quasi-TM mode, end ported MMI, where the letter V represents the V region.

shown in Fig. 1(a), a triangle region, in which the TE light intensity is notably low, is highlighted by red dashed line and is termed as V region hereafter. By putting the TM output waveguide at the V region, only very little TE light power could leak into the TM output waveguide, thus, separating the TE and TM lights.

Fig. 2(a) shows the schematic structure of the proposed PBS. The length of MMI1 $L_{MMI1} = L_{TM}$. A second MMI2 is cascaded with MMI1 in its left region to collect the reflected TE light power. Different from the end ported devices in Ref. [9], in which the access waveguides are placed on back and front ends of MMIs, the input and output waveguides are positioned on the side walls of MMIs. As shown in Fig. 2(a), there is an angle θ_{in} between the access waveguide and the MMI side walls. $\theta_{in} = 8°$ in this paper if not specified. Fig. 2(b) shows the cross-section structure of the waveguide studied in this work. The waveguide's core layer is a 300 nm thick InGaAsP material with a 1.2 μm bandgap wavelength. The thickness of the InP cap layer is 1.5 μm. The total height of the ridge waveguide is 2.6 μm. The refractive indexes are 3.206 and 3.424 for InP and InGaAsP materials, respectively, and the working wavelength is 1310 nm. Three-dimension (3D) beam propagation method (BPM) is used to simulate the light propagations. The ER and IL of the PBS are defined as:

$$ER = -10\log(P_d/P_u) \tag{3}$$

$$IL = -10\log(P_d/P_{in}) \tag{4}$$

where P_d and P_u are the intensities in the desired and undesirable output ports respectively, and P_{in} is the intensity in the input waveguide. As will be shown in detail in the following, the side ported access waveguides enhance the performance of the PBS greatly. This can be attributed to their effects on the properties of the V region described in Fig. 1. Due to the different self-imaging process, the light intensity distribution is also different. Compared with the end ported MMI with same MMI width and access waveguide width, the side ported MMI shows much lower light intensity distribution in the V region, as can be seen from Fig. 1 by comparing Fig. 1(a) and (b) with Fig. 1(c) and (d). On the one hand, because the TM mode output waveguide can be placed at a cleaner V region, less TE power will be coupled into the TM output, which leads to a higher ER. On the other hand, the TE mode's light power can be collected effectively by the collecting MMI with a narrow width, which lowers the ILs.

For the end ported PBS, the width of the main MMI must be increased to obtain better performance [9], which will also increase the length of the MMI greatly because the MMI length is proportional to the square of its width. A wider collecting MMI also must be used to collect more TE power, which, however, results in a lower ER. It is because that the separation between the TM output waveguide and the collecting MMI is reduced at the same time, which will increase the crosstalk between TE and TM modes. Besides, the difference between L_{TM} and L_{TE} of the side ported MMI is larger than the difference of the end ported MMI. As a result, the TM output waveguide of side ported PBS is more far away from the image point of TE mode, further reducing the crosstalk.

Fig. 3 shows the TE and TM light propagations in a side ported PBS at 1.31 μm. The width of the input/output waveguides is $W_{out} = 1.0$ μm. The widths of MMI1 and MMI2 are $W_{mmi1} = 4.5$ μm and $W_{mmi2} = 2.5$ μm, respectively. The corresponding lengths are $L_{mmi1} = 240$ μm and $L_{mmi2} = 59.2$ μm, respectively, resulting a PBS length of 299.2 μm. The gap width between the TM output waveguide and the collecting MMI is 2 μm. The ER and IL of the TE and TM modes are about 37.8 dB and 0.6 dB, 31.4 dB and 0.1 dB, respectively. For comparison, the properties of an end ported PBS, which has the same MMI1 width as that of the side ported PBS, are also calculated. The lengths of its MMI1 and MMI2 are 224.5 μm and 64.2 μm, respectively, leading to a total length of 288.7 μm. As shown in Fig. 4(a) and (b), The ER and IL at 1310 nm of the TE and TM modes are about 9.4 dB and 1 dB, 23.1 dB and 0.21 dB, respectively, all of which are worse than the corresponding values of the side ported PBS. It also should be noticed that the difference between L_{TE} and L_{TM} increases with the width of MMI, which helps to enhance the performance of PBS. As shown in Ref. [9], when the width of MMI1 of the end ported PBS is increased to 8 μm, though the TM mode ER can be increased to be over 30 dB, the TE mode ER is still only about 21 dB. The large MMI length results in a PBS length of 950 μm which is over three times of the length of the side ported one. To further improve the TE mode ER, an MMI filter can be used [9], which however complicates the device structure.

The ERs and ILs at different wavelengths of the side and end ported PBSs both having $W_{mmi1} = 4.5$ μm are shown in Fig. 4(a) and (b), respectively. For the side ported PBS, the TM mode ER is larger than 20 dB in the wavelength range from 1289 nm to 1328 nm and the TE mode ER exceeds 20 dB in the wavelength range from 1291 nm to 1321 nm. For the end PBS, however, only the TM mode ER is larger than 20 dB in a narrow wavelength range from 1306 nm to 1315 nm. The TE mode ER is smaller than 10 dB for all the wavelengths. The ILs for both the PBS is smaller than 4.3 dB in the wavelength range from 1295 nm to 1325 nm.

θ_{in} in Fig. 2 is an important parameter for the design of the side ported PBS. θ_{in} dependence of the IL and ER of the side ported PBS at 1310 nm is shown in Fig. 5(a) and (b), respectively. As can be seen from Fig. 5(a), the TE and TM ER increase with θ_{in} and peaks at 7 and 8 degree, respectively. Increase of θ_{in} to 9 degree leads to ER decrease for both modes. At further larger angles, no stable mode propagation is supported in the PBS waveguide. As can be seen from Fig. 5(b), while the TM mode IL keeps below 0.16 dB in the angle range, the TE mode IL decreases gradually.

The effects of the width of MMI2 on the ER and IL of the side ported PBS are shown in Fig. 6. Because of the clean V region, the TE mode power can be collected by MMI2 effectively. Even when MMI2 has less than half the width of MMI1, the TE mode's IL is less than 1 dB. The TE mode's ER is better than 30 dB when the width of MMI2 is varied

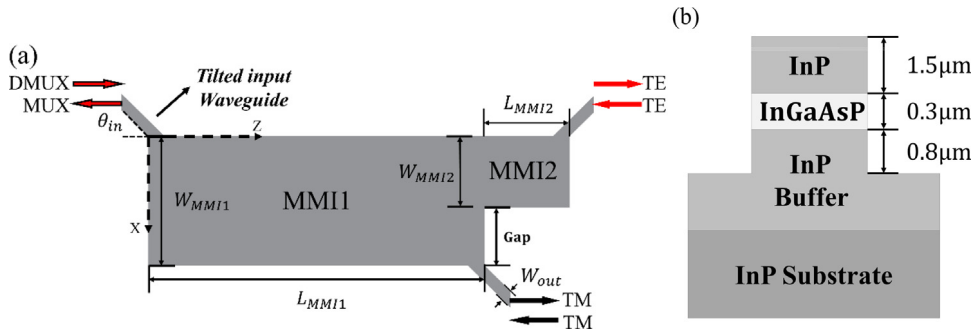

Fig. 2. Schematic configuration of the PBS structure (a) top view; (b) cross section view.

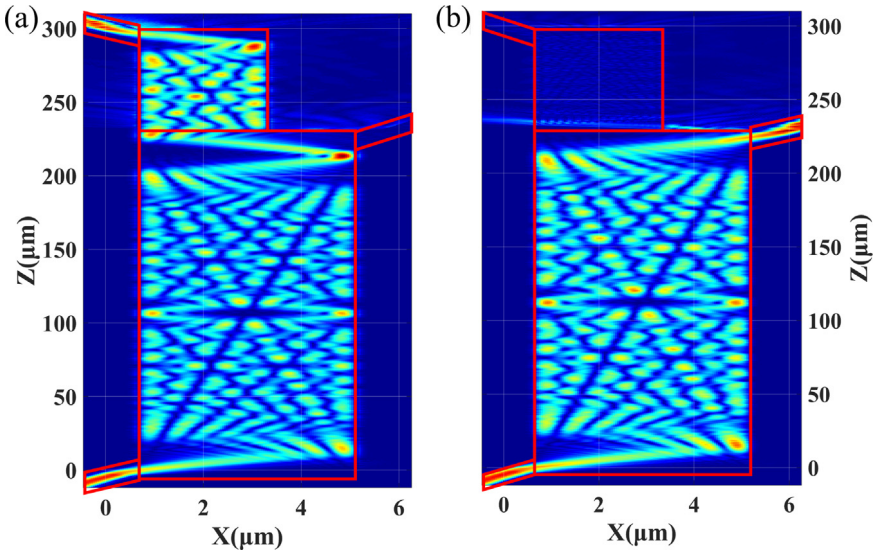

Fig. 3. Propagations of lights at 1310 nm in the side ported PBs in quasi-TE mode (a) and quasi-TM mode (b).

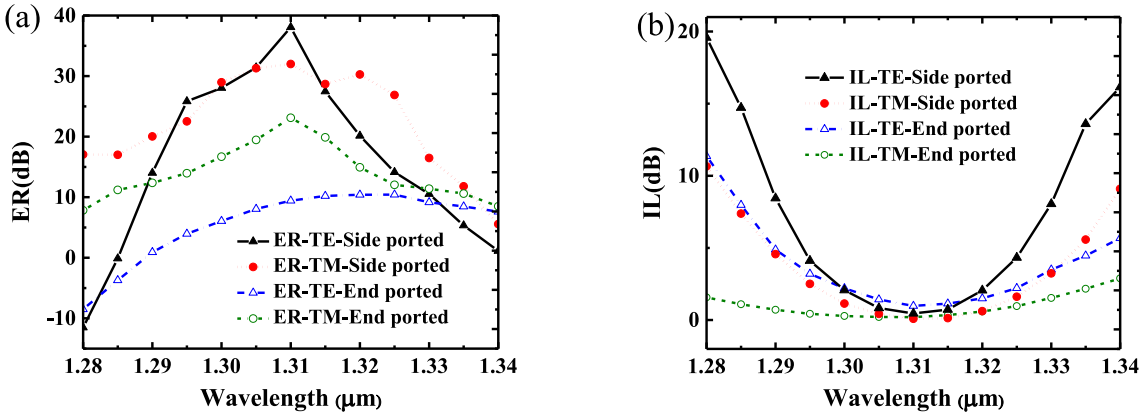

Fig. 4. ERs (a) and ILs (b) of the PBSs at TE and TM polarizations as a function of wavelength.

from 2.0 μm to 3.7 μm. As can be seen from Fig. 6(a), the TM mode's ER decreases notably when the width of MMI2 is larger than 3.1 μm, it is because that the TM mode power starts to be coupled into MMI2. It also can be seen than the IL of the TE mode decreases simultaneously when the width of MMI2 is larger than 3.1 μm, which can be explained by the fact that a larger MMI2 can collect more TE mode light, resulting in a lower loss of the TE mode.

For the end ported PBS, the effects of the width of MMI2 on the ER and IL are also simulated. The width of the input/output waveguides is 1.0 μm. The widths of MMI1 and MMI2 are 4.5 μm and 2.5 μm, and the lengths of MMI1 and MMI2 are 224.5 μm and 64.2 μm, respectively. As shown in Fig. 7, the TE mode only has less than 10 dB ER. To reduce the TE mode IR below 1 dB, the width of MMI2 must be increased over 3.4 μm to collect more light power. It is even worse that width like this would lead to only 100 nm separation between MMI2 and the TM output ports, which is difficult to be realized experimentally. In comparison, for the side ported PBS, the separation between MMI2 and the TM output ports can be set as large as 2 μm without damaging either ERs or IRs significantly, which eases device fabrication greatly. Finally, we would like to point out that tapered input and output waveguides do not help to improve the performance of the PBSs.

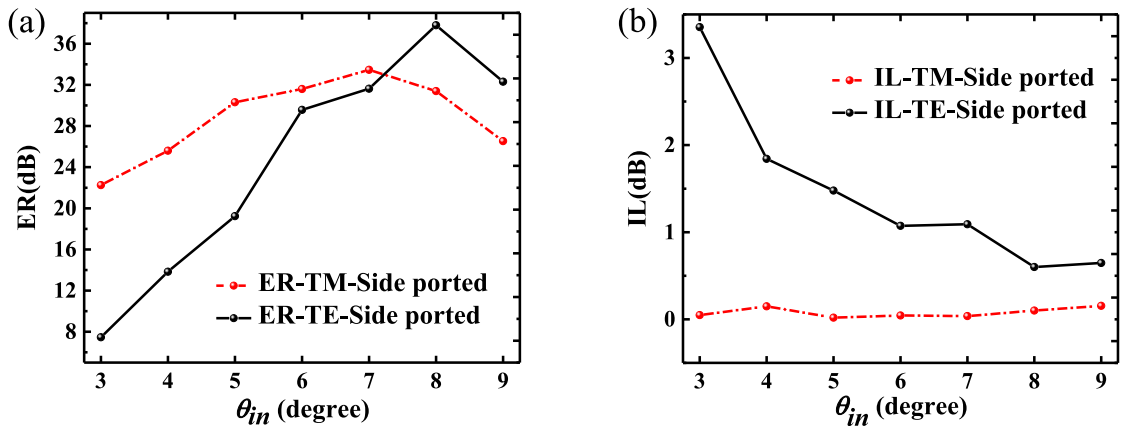

Fig. 5. ERs (a) and ILs (b) of the side ported PBS as a function of the θ_{in} at 1310 nm.

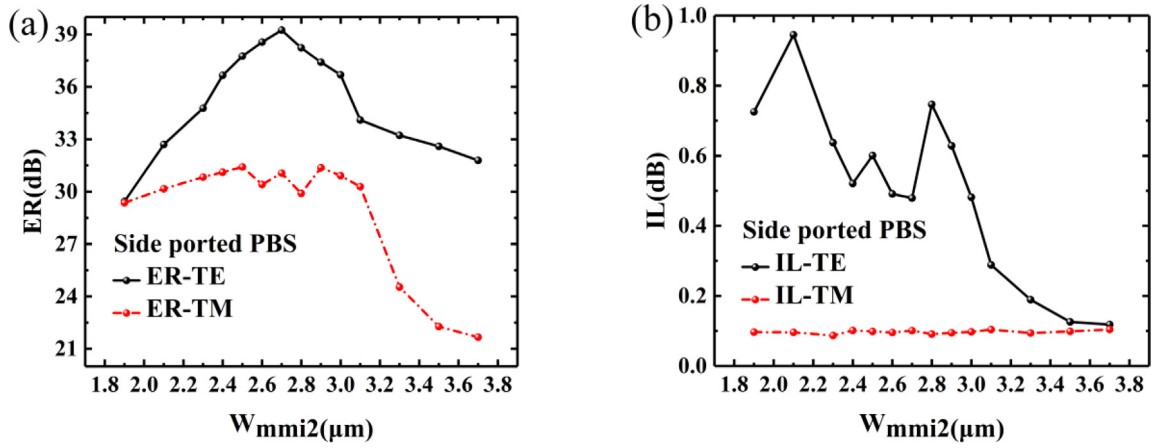

Fig. 6. ERs (a) and ILs (b) of the side ported PBS as a function of the width of MMI2 at 1310 nm.

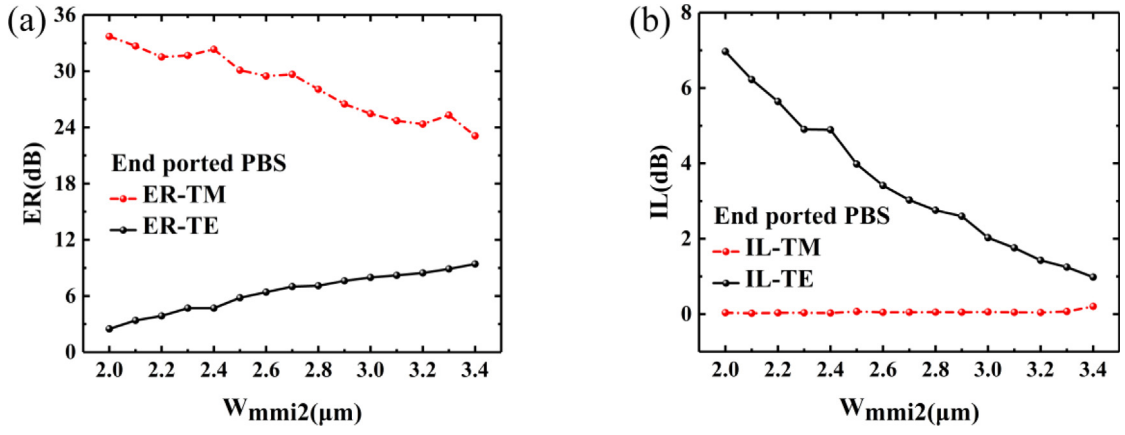

Fig. 7. ERs (a) and ILs (b) of the end ported PBS as a function of the width of MMI2 at 1310 nm.

3. Conclusions

In summary, by placing the input and output waveguides on side walls of the PBS MMIs, the length of the PBS can be shortened effectively, while maintaining both low IL and high ER. For the optimized PBS design, the length of the side ported PBS is 299 μm, which is only 1/3 of the length of the end ported PBS. This PBS is promising for applications in future high performance InP based PICs.

Declaration of competing interest

The authors declare that they have no known competing financial interests or personal relationships that could have appeared to influence the work reported in this paper.

Acknowledgments

This manuscript is not published anywhere and have not any intention to submit it to another publication. The authors whom are participated in this research are thankful for their participation.

Funding

This work was supported by the National Natural Science Foundation of China [grant numbers 61635010, 61320106013]; the National Key Research and Development Program of China [grant number 2018YFB2200801].

References

[1] F.A. Kish, D. Welch, R. Nagarajan, J.L. Pleumeekers, V. Lal, M. Ziari, et al., Current status of large-scale InP photonic integrated circuits, IEEE J. Sel. Top. Quantum Electron. 17 (6) (2011) 1470–1489, http://dx.doi.org/10.1109/JSTQE.2011.2114873.

[2] T. Barwicz, M.R. Watts, M.A. Popovi, P.T. Rakich, L. Socci, F.X. Kärtner, et al., Polarization-transparent microphotonic devices in the strong confinement limit, Nat. Photonics 1 (1) (2007) 57–60, http://dx.doi.org/10.1038/nphoton.2006.41.

[3] J. Xu, S. Liang, Z. Zhang, J. An, H. Zhu, W. Wang, EML array fabricated by SAG technique monolithically integrated with a buried ridge AWG multiplexer, Opt. Laser Technol. 91 (2016) (2017) 46–50, http://dx.doi.org/10.1016/j.optlastec.2016.12.010.

[4] E.A. El-Fiky, A. Samani, D. Patel, D.V. Plant, A high extinction ratio, broadband, and compact polarization beam splitter enabled by cascaded MMIs on silicon-on-insulator, in: 2016 Optical Fiber Communications Conference and Exhibition, OFC, 2016, pp. 1–3, http://dx.doi.org/10.1364/ofc.2016.w2a.8.

[5] K.W. Chang, C.C. Huang, Ultrashort broadband polarization beam splitter based on a combined hybrid plasmonic waveguide, Sci. Rep. 6 (2015) (2016) 1–11, http://dx.doi.org/10.1038/srep19609.

[6] M.S. Lai, C.C. Huang, Submicron-scale broadband polarization beam splitter using CMOS-compatible materials, Sci. Rep. 7 (1) (2017) 1–8, http://dx.doi.org/10.1038/s41598-017-05019-3.

[7] D. Pérez-Galacho, R. Halir, A. Ortega-Moñux, C. Alonso-Ramos, R. Zhang, P. Runge, et al., Integrated polarization beam splitter with relaxed fabrication tolerances, Opt. Express 21 (12) (2013) 14146, http://dx.doi.org/10.1364/oe.21.014146.

[8] S. Keyvaninia, H. Boerma, M. Wössner, F. Ganzer, P. Runge, M. Schell, Highly efficient passive inp polarization rotator-splitter, Opt. Express 27 (18) (2019) 25872, http://dx.doi.org/10.1364/oe.27.025872.

[9] L. Han, S. Liang, H. Zhu, C. Zhang, W. Wang, A high extinction ratio polarization beam splitter with MMI couplers on InP substrate, IEEE Photonics Technol. Lett. 27 (7) (2015) 782–785, http://dx.doi.org/10.1109/LPT.2015.2392383.

[10] N. Abadía, X. Dai, Q. Lu, W.-H. Guo, D. Patel, D.V. Plant, J.F. Donegan, Highly fabrication tolerant InP based polarization beam splitter based on $p-i-n$ structure, Opt. Express 25 (9) (2017) 10070, http://dx.doi.org/10.1364/oe.25.010070.

[11] L.M. Augustin, J.J.G.M. van der Tol, R. Hanfoug, W.J.M. de Laat, M.J.E. van de Moosdijk, P.W.L. van Dijk, et al., A single etch-step fabrication-tolerant polarization splitter, J. Lightwave Technol. 25 (3) (2007) 740–746, http://dx.doi.org/10.1109/JLT.2006.890430.

[12] N. Zhao, C. Qiu, Y. He, Y. Zhang, Y. Su, Broadband polarization beam splitter by using cascaded tapered bent directional couplers, IEEE Photonics J. 11 (4) (2019) http://dx.doi.org/10.1109/JPHOT.2019.2920909.

[13] D. Dai, Z. Wang, J. Peters, J.E. Bowers, Compact polarization beam splitter using an asymmetrical Mach–Zehnder interferometer based on silicon-on-insulator waveguides, IEEE Photonics Technol. Lett. 24 (8) (2012) 673–675, http://dx.doi.org/10.1109/LPT.2012.2184530.

[14] X. Dai, G. Zhao, Q. Chen, Q. Lu, J.F. Donegan, W. Guo, High-performance InP-based Mach–Zehnder polarization beam splitter with a 19 dB extinction ratio across C-band, Opt. Lett. 44 (17) (2019) 4299, http://dx.doi.org/10.1364/ol.44.004299.

[15] L. Xu, Y. Wang, E. El-Fiky, D. Mao, A. Kumar, Z. Xing, et al., Compact broadband polarization beam splitter based on multimode interference coupler with internal photonic crystal for the SOI platform, J. Lightwave Technol. 37 (4) (2019) 1231–1240, http://dx.doi.org/10.1109/JLT.2018.2890718.